AIAA 81-4186

Analysis of Boundary Layers on Perforated Walls of Transonic Wind Tunnels

Y.Y. Chan*
National Research Council of Canada, Ottawa, Canada

The boundary-layer development on the perforated walls of a transonic wind tunnel has been studied experimentally under model testing conditions for a better understanding of the flow characteristics from which a proper boundary condition for wall interference calculations could be formulated. The results show that the boundary-layer effect is small for the portion of the wall with outflow. With inflow, however, the wall characteristics are highly nonlinear and strongly modulated by the boundary layer. The normal velocity induced by the displacement effect can be up to three times as great as the inflow velocity at the wall. The wall characteristics, the boundary-layer development, and the inviscid interference flow are all interdependent and must be solved together as a single problem.

Nomenclature

c = chord length of airfoil model
C_L = lift coefficient
C_p = pressure coefficient
d = hole diameter of the perforated wall
H = form factor
M = Mach number
U, V = velocity components in x,y directions, respectively
x, y = Cartesian coordinates
α = angle of attack
δ^* = displacement thickness
ϑ = momentum thickness
ρ = density

Subscripts

e = condition at the edge of the boundary layer
w = condition at the wall

I. Introduction

THE requirement of minimizing the wind-tunnel wall interference at transonic speeds has led to a new surge of research activities in recent years. The characteristics of the tunnel walls of existing wind tunnels have been carefully reexamined[1] and the new concepts of self-correction[2] and correctable interference[3] have been introduced. In order to calculate the flow in the test section properly, the characteristics of the tunnel wall must be precisely defined to provide the boundary conditions. For a tunnel with perforated walls it is normally assumed that the normal velocity of the inflow and outflow at the wall are linearly proportional to the local pressure difference between the test section and the plenum chamber.[4,5] The proportional constant is the porosity factor which depends on the physical configuration of the wall. This linear relation has been accepted for wall-interference calculations for many years, however it holds true only in relatively low-speed flows.[6] As the Mach number increases toward the transonic range, some nonlinear characteristics can be readily observed.[7,8] It should also be noted that these early experiments measured the average mass flow over the tunnel wall in an empty tunnel. In real model testing conditions, the pressure field generated by the model will induce a complicated variation of crossflow along the walls. The wall characteristics in such a condition were recently investigated.[1] The results indicate that the pressure-crossflow relation at the wall is far from linear. It depends on the pressure distribution and the local boundary-layer thickness at the wall.

In the earlier experiments[8,9] some of the nonlinear wall throughflow characteristics observed were found to be due to boundary-layer development. The detailed measurements of the local flow at the wall in Ref. 1 firmly established the importance of the boundary layer and showed that the mean slope of the nonlinear wall characteristics could be correlated to the averaged displacement thickness along the wall. The boundary-layer development along the wall, on the other hand, depends on the wall characteristics. Thus we face a mutually interacting problem in the determination of the flow over the perforated wall.

The development of a boundary layer along the wall not only modulates the wall characteristics, but also induces a displacement of the external inviscid flow. The amount of displacement is directly related to the rate of growth of the boundary layer, which can be quite appreciable if inflow is dominant. The displacement effect must be added to the wall characteristics in establishing the boundary condition for the interference calculation. It is clear that the wall characteristics, the boundary layer, and the inviscid interference flowfield are interrelated, with the boundary layer playing a dominant role. Thus detailed studies of the boundary-layer development are deemed necessary and the present investigation has been conducted with this understanding.

In the present study, the boundary layer along the perforated wall was measured under transonic testing conditions, with the pressure field generated by a model. In between the measuring stations, a computation code was employed to fill in the boundary layer flow, giving finer detail for the evaluation of the displacement effect and the wall characteristics. The results show that for positive lift, the lower wall is dominated by outflow and the boundary-layer effect is small. The upper wall has both outflow and inflow and the displacement effect induces a normal velocity appreciably larger than that at the wall. The resulting pressure-normal velocity relation is highly nonlinear. The wall characteristics are strongly modulated by the boundary layer and a correlation depending explicitly on the displacement thickness is obtained.

The experiment was performed in a transonic wind tunnel with a specific wall configuration and the data obtained thus depend on the parameters of that configuration. However, since the present study emphasizes the understanding of the mechanism of the interaction of different elements in the flowfield, the observations thus made can be applied to flows past a porous wall in a more general sense. The empirical coefficients derived from the data are, of course, parametric

Received July 11, 1980; revision received Feb. 4, 1981.

*Senior Research Officer, High Speed Aerodynamics Laboratory. Member AIAA.

dependent. The correlations of the flow elements however can be considered as general.

II. Experiments

The experiments were performed in the National Aeronautical Establishment two-dimensional test facility.[10] The two-dimensional working section has a width of 15 in. and a height of 60 in. The top and bottom walls are parts of the 5 ft^2 transonic section and are perforated with 0.5 in. diam normal holes at 1.04 in. centers in staggered rows, giving a porosity of 20.5%. The thickness of the perforated wall is 0.5 in. The test model was 10 in. in chord and had a BGK 1 transonic profile.[11] A static pressure pipe of 1 in. diam was mounted along the centerline of the top and the bottom walls, respectively, for the measurement of the static pressure variation along the walls.

The turbulent boundary layers were measured by pitot rakes of hypodermic tubings finished with square ends. The pitot tubes were connected to a scanivalve and the pressure was measured by a Kulite transducer of 200 psia range. The boundary-layer rakes were mounted at the top and the bottom walls at a position half-way between the side wall and the static pressure pipe. For the upper wall, measurements were taken at three stations located at $x/c = -1.5$, -0.025, and 1.65 with respect to the origin designated at 0.4 chord length from the leading edge of the model (x positive in the stream direction). For the lower wall, only one station at $x/c = -0.025$ was measured.

The experiments were performed at a series of Mach numbers ranging 0.5–0.8. The Reynolds number was set at a value of 21.5×10^6 per chord. For each Mach number, the angle of attack of the model varied within a range of -3.5 to 11.8 deg. The Mach number distribution across the boundary layer was calculated from the pitot pressures measured by the rake and the static pressure from the centerline static pipe, interpolated to the pitot rake position. The velocity distribution was then calculated assuming van Driest's form of temperature distribution.[12] The wall was assumed to be insulated and the recovery factor taken to be 0.89. A detailed report of the experiments and the resulting data are given in Ref. 13.

III. Experimental Results

Boundary-Layer Measurements

The boundary-layer development along the perforated wall depends mainly on the inflow and outflow through the wall, which is generated by the pressure difference between the plenum and the local condition in the test section. Thus the static pressure variation along the wall is the basic factor controlling the growth of the boundary layer. Some typical static pressure distributions at both the upper and lower walls for Mach number 0.7 and a range of angles of attack are shown in Fig. 1. With positive lift, the pressure coefficient at the lower wall is always positive, while at the upper wall it starts with a slight positive dip and then becomes negative downstream.

At low angles of attack, boundary layers can be observed on both walls. As the angle of attack increases, the pressure increases rapidly at the lower wall and causes a strong outflow. The boundary-layer thickness decreases rapidly and eventually cannot be detected by the pitot rake. The boundary-layer integrated properties, the displacement thickness δ^*, the momentum thickness θ (normalized by the hole diameter), and the form factor H of the perforated wall are shown as a function of the lift coefficients C_L in Fig. 2. For C_L greater than 0.6, the measurements show a very small velocity deficit and the integrated thicknesses approach zero. (The finite value shown in the graph is the limit of the accuracy of the experiment.) This indicates that the boundary layer is bled completely from the lower wall. At lower values of C_L, a thin boundary layer can be observed with its growth rate inhibited by the outflow. Thus at the lower wall the boundary-layer effect is small and is negligible at moderate- and high-lift conditions.

The upper wall, on the other hand, has a much more complicated boundary-layer development than that of the lower wall. The positive pressure coefficient upstream causes outflow and thinning of the boundary layer. The negative pressure coefficient sets in at about $x/c = -2.5$ and the rest of the wall is then dominated by inflow, causing rapid thickening of the boundary layer. As shown in Fig. 3, the boundary layer grows rather slowly between the first and the second measuring stations, and then rapidly toward the third station. It is noted that the growth rates of the boundary layer as measured at these three stations do not follow directly the variation of the pressure coefficient which controls the inflow and outflow. Between stations 1 and 2, the pressure coefficient is negative (see Fig. 1). If the inflow is directly proportional to the pressure coefficient as assumed by the linear wall characteristics, one would expect the boundary layer to grow much faster than is shown in the measurements. Between stations 2 and 3, again if the linear relation applies, the inflow will have a near constant value approximately the same as that at the rear half of the first measuring section. It is expected that a steady growth rate similar to the rear part of the preceding boundary layer would occur. However, the data show a continuous increase of growth rate to a value much larger than that at the second measuring station. This suggests that the inflow is not only a function of the pressure distribution but is also modulated by the boundary-layer growth.

The distribution of experimental data on the boundary-layer development along the wall is too coarse in this case for an accurate evaluation of the displacement effect and the wall characteristics. Thus, in between the measuring stations the boundary-layer development is obtained by computation based on a computer code.[14] This gives finer details of the

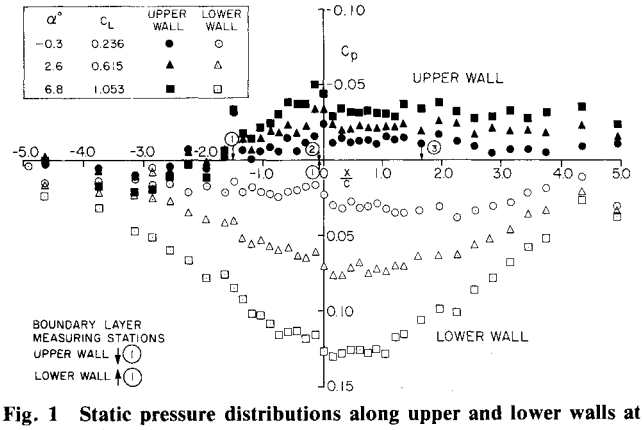

Fig. 1 Static pressure distributions along upper and lower walls at Mach 0.703.

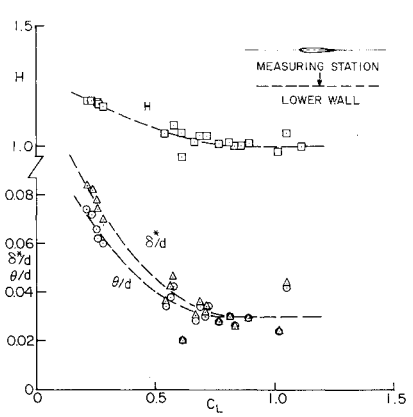

Fig. 2 Boundary-layer properties at lower wall.

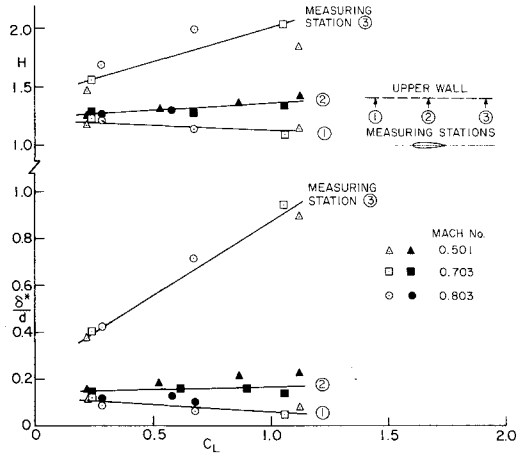

Fig. 3 Boundary-layer developments at upper wall.

boundary layer and allows the evaluation of the desired information with required accuracy. In the following discussion the development along the upper wall will be emphasized because of its complicated crossflow distributions.

Boundary-Layer Calculations

The boundary-layer computation code is based on a differential method with the turbulent kinetic energy expressed in terms of an extended mixing length.[14] The code calculates the boundary-layer development under arbitrary external pressure gradient and surface mass-transfer distributions. For a given initial condition, the boundary-layer development depends on the external pressure distribution and the suction or injection velocity at the wall. For the present calculations, the velocity profile measured at the first station is used for the initial condition. The external pressure distribution is provided by the static pipe measurements as shown in Fig. 1. The experimental data indicate that the boundary-layer thickness ranges about 0.5-1.5 in. in the region of interest. The static pressure measured at 1 in. away from the wall by the static pipe would provide a reasonable approximation for the external pressure as the pressure gradient normal to the flow direction is very small near the wall. The static pressure is assumed to be constant across the boundary layer. The suction or injection velocity variation at the wall depends on the wall characteristics as yet unknown. To deduce the wall characteristics from the experimental data, a model is first constructed so that the local mass flow across the wall is a function of the pressure coefficient and the displacement thickness. With this model, the boundary layer can be calculated from the first station through the second and then to the third. The calculated velocity profiles at the second and third stations are then compared with the measured ones. The wall characteristics model is adjusted until a satisfactory match of the velocity profiles is obtained. This is essentially curve fitting through the data points along the wall with the computed solutions yielding the details of the boundary-layer development and the wall characteristics. The details of the boundary-layer computation can be found in Ref. 13.

Six cases were chosen for the boundary-layer calculations, three with low lift and three with high lift. The conditions of these cases are listed in Table 1. These cases cover the pressure distributions for both high and low lift. The range of Mach number considered is wide enough to detect any parametric dependency.

IV. Displacement Effects and Wall Characteristics

The wall characteristics for the cases considered are shown in Fig. 4. The normal velocity at the wall in the form of local mass flow ratio $\rho_w V_w/\rho_e U_e$ is plotted against the local pressure coefficient. Each curve depends on the local pressure distribution and does not follow a simple linear law. The

Table 1 Cases chosen for boundary-layer calculations

M	α, deg	C_L	α, deg	C_L
0.501	−0.3	0.218	8.8	1.118
0.703	−0.3	0.236	6.8	1.053
0.803	−0.4	0.282	3.5	0.675

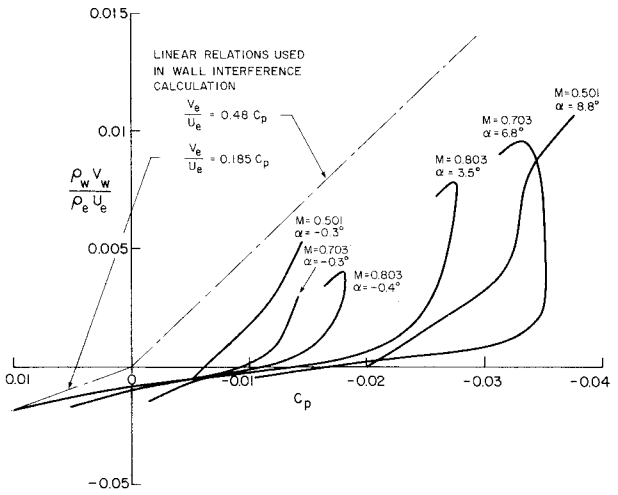

Fig. 4 Mass flow variation at upper wall.

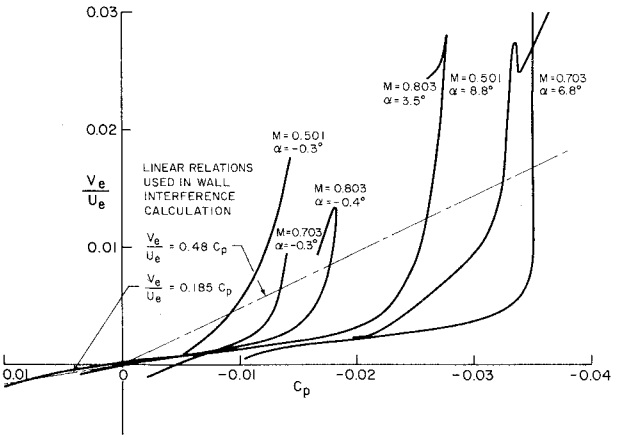

Fig. 5 Normal velocities at edge of boundary layer, upper wall.

behavior of the curves follows closely those of Ref. 1 which were obtained from direct measurements. These curves do not pass through the origin and the slope for the inflow portion (positive v_w) is generally much greater than that of the outflow. This confirms our observations discussed in Sec. III that the inflow or outflow is not only a function of the pressure distribution, but is also modulated by the local boundary-layer properties. The offsetting of the curves from passing through the origin of the coordinates indicates that the crossflow through the perforated hole depends on the local velocity gradient. The local flowfield near the hole can no longer be considered as a simple uniform potential flow[6] but as a rotational shear flow.

The normal velocity at the edge of the boundary layer includes the displacement effect and the mass transfer at the wall, and can be written as[15]

$$\frac{V_e}{U_e} = \frac{1}{\rho_e U_e}\frac{\mathrm{d}}{\mathrm{d}x}(\rho_e U_e \delta^*) + \frac{\rho_w V_w}{\rho_e U_e} \tag{1}$$

The normal velocity V_e/U_e for these cases is shown in Fig. 5 as a function of pressure coefficient C_p. In comparison with the wall characteristics shown in Fig. 4, the displacement

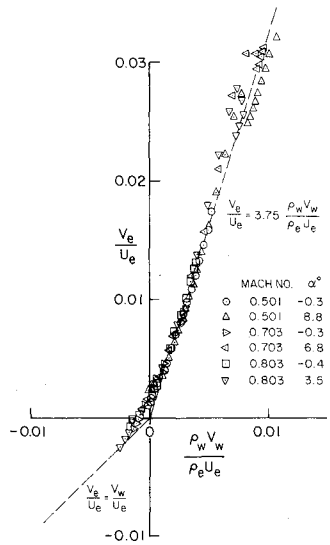

Fig. 6 Correlation of normal velocity at edge of boundary layer to mass flow at wall.

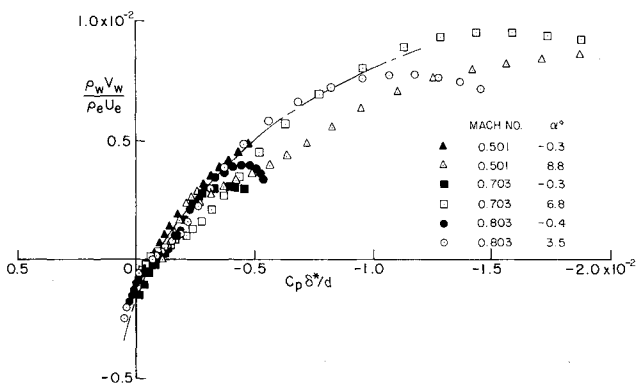

Fig. 7 Correlation of wall characteristics, $\delta^*/d \leq 0.25$.

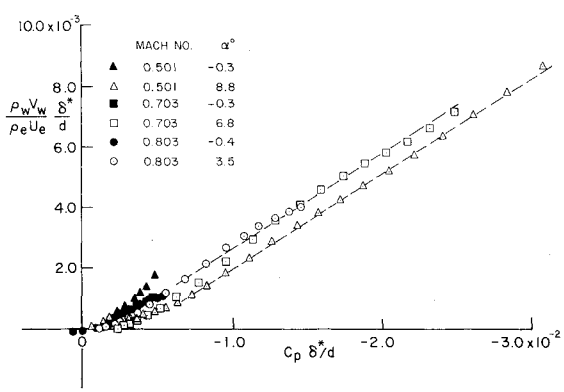

Fig. 8 Correlation of wall characteristics, $\delta^*/d \geq 0.25$.

effect not only moves the curves upward but also amplifies the local values. (Note the difference in ordinate scale.) With inflow the induced velocity can be as much as three times greater than that at the wall. The curves are nonlinear and similar to those of the wall characteristics.

The linear relations assumed for the boundary condition in classical wall interference calculations are also shown in Fig. 5 for comparison. The corresponding porosity factors are the averaged values for the cases considered and have values of 0.96 and 0.37 for the upper and lower walls, respectively.[16] These values are deduced by fitting the calculated interference wall pressure distributions to the experimental data.[17] It is interesting to observe that the linear relation does pass through all nonlinear curves and presents an averaging trend of the functional relationship of V_e/U_e and C_p. However, the linear relation fails to reproduce the local value of the normal velocity correctly. Since the normal velocity is the output of the boundary condition for the wall interference calculation, large errors might result if the linear relation is assumed. The linear relations are also plotted in Fig. 4, showing a trend much higher than the wall characteristics. It demonstrates that the displacement effect must be taken into account in addition to the wall characteristics in the real flow situation.

The nearly exponential increase of the inflow velocity along the wall suggests that this portion of the boundary layer is close to equilibrium. Thus a similarity correlation can be established between the induced velocity at the edge and the mass transfer at the wall as shown in Fig. 6. The correlation can be approximated by a straight line

$$\frac{V_e}{U_e} = 3.25 \frac{\rho_w V_w}{\rho_e U_e} \tag{2}$$

for the injection side. At the suction side the correlation approaches a direct relation asymptotically.

$$\frac{V_e}{U_e} = \frac{V_w}{U_e} \tag{3}$$

as the $d\delta^*/dx$ is small in comparison with the suction velocity. The linear boundary conditions discussed in Fig. 5 assume a porosity factor for the upper wall about three times greater than that of the lower wall. This is obviously related to the different natures of the boundary-layer growth on the respective walls and is reflected by the correlation coefficients of the boundary layer.

The wall characteristics shown in Fig. 4 depend not only on the pressure distribution, but also on the boundary-layer development. By taking the variation of the displacement thickness into account, the wall characteristics can be correlated as shown in Fig. 7. For each case considered, the data follow a common correlation curve to a certain point and then branch off. All cases indicate that at the branching-off point, the value of δ^*/d is about 0.25, and the ratio of the boundary-layer thickness δ to the hole diameter d has a value of about 1 or greater. Thus, for δ^*/d less than 0.25, the wall characteristics can be correlated by the envelope of the data as shown, the correlation can be approximated by a quadratic

$$\frac{\rho_w V_w}{\rho_e U_e} = -2.78(\xi - \xi_0) - 201.5(\xi - \xi_0)^2, \quad 0 \leq \frac{\delta^*}{d} \leq 0.25 \tag{4}$$

where $\xi = C_p \delta^*/d$ and $\xi_0 = -0.0004$.

When the boundary-layer thickness is greater than the hole diameter, the dependence of the wall characteristics on the boundary layer is reduced and the data can be correlated in a different form as shown in Fig. 8. For δ^*/d greater than 0.25, the correlations appear to be linear and have the same slope. The empirical relation can be written as

$$\frac{\rho_w V_w}{\rho_e U_e} = -0.316\left[C_p - \frac{(C_p \delta^*/d)_0}{\delta^*/d}\right] + \left[\frac{\rho_w V_w}{\rho_e U_e}\frac{\delta^*}{d}\right]_0 \frac{d}{\delta^*}, \quad \frac{\delta^*}{d} \geq 0.25 \tag{5}$$

where the subscript 0 refers to the point at $\delta^*/d = 0.25$. This correlation shows that as the mass flow at the wall increases, it becomes less dependent on δ^*/d and asymptotically approaches the inviscid form in the limit. The empirical constants appearing in the correlations depend on the configuration of the wall. The functional relations of the correlations, however, should be general. The scattering of the data for these two correlations can be further reduced by including the rate of growth of the displacement thickness δ^*,

in the form $C_p \cdot \delta^*/d \cdot d\delta^*/dx$. The effect is of second order and does not change the general features of the wall characteristics.

One can now observe that the flow past a perforated wall consists of a problem of strong interaction between the wall, the boundary layer, and the external inviscid flow induced by the model. To establish the boundary condition for the interference calculation, the interdependent relations of the wall characteristics and the boundary layer must be solved. These relations are in turn explicitly dependent on the pressure distributions at the wall which is a part of the solution of the interference problem. Therefore one can no longer consider the wall conditions separately in the interference calculation, but must include them as an integral part of the problem to be solved.

The linear relation of V_e/U_e vs C_p normally used in the interference calculation averages out the variation along the wall. With a different porosity factor for the upper and lower walls, respectively, the linear relation provides a first rough approximation of the boundary-layer displacement effect on the characteristics of the two walls. However, for an accurate representation of the wall characteristics, the nonlinear nature must be considered.

V. Conclusions

The development of the boundary layer on the perforated walls of a transonic wind tunnel has been studied experimentally under model testing conditions. The effect of the displacement of the boundary layer and the wall characteristics are examined to provide a better understanding of the flow at the wall. The results of the present study can be summarized as follows:

1) The pressure coefficient distributions at the lower wall are positive for cases with positive lift, causing outflow through the wall. The boundary-layer displacement effect is small and can be neglected for cases with moderate and high lift. A linear pressure-normal velocity wall characteristic can be assumed.

2) For the upper wall, the pressure is slightly positive upstream and changes to negative downstream, causing inflow and then outflow with the latter dominating. The crossflow velocity at the wall is a nonlinear function of the pressure coefficient because of the strong modulation caused by the boundary-layer development. Wall characteristics in terms of crossflow velocity as a function of pressure coefficient and normalized displacement thickness can be correlated universally.

3) The normal velocity induced by the growth of the boundary layer can be three times as great as the inflow velocity at the wall. The displacement effect must be considered for the portion of boundary layer with inflow at the wall.

4) The linear relation of V_e/U_e vs C_p, normally employed in the boundary conditions of the wall interference calculation, does not adequately represent the real flow. The boundary condition can be established only by solving the interdependent relations of the wall characteristics and the boundary-layer development. These relations are in turn controlled by the wall pressure distribution which is part of the solution of the interference calculation. Thus the flow over the perforated walls must be considered as an integral part of the tunnel flow and treated simultaneously with the inviscid flow calculation in the test section.

References

[1] Jacocks, J.L., "An Investigation of the Aerodynamic Characteristics of Ventilated Test Section Walls for Transonic Wind Tunnels," Ph.D. Dissertation, University of Tennessee, Knoxville, Dec. 1976.

[2] Vidal, R.J., Ericson, J.C. Jr., and Catlin, P.A., "Experiments with a Self-Correcting Wind Tunnel," *Wind Tunnel Design and Testing Techniques,* AGARD-CP-174, Oct. 1975.

[3] Kemp, W.B. Jr., "Toward the Correctable-Interference Transonic Wind Tunnel," *Proceedings of AIAA Ninth Aerodynamic Testing Conference,* June 1978, pp. 31–38.

[4] Baldwin, B.S. Jr., Turner, J.B., and Knechtel, E.D., "Wall Interference in Wind Tunnels with Slotted and Porous Boundaries at Subsonic Speeds," NACA TN 3176, May 1954.

[5] Goodman, T.R., "The Porous Wall Wind Tunnel: Part II, Interference Effect on a Cylindrical Body in a Two-Dimensional Tunnel at Subsonic Speeds," Cornell Aeronautical Laboratory Rept. AD-594-A-3, Nov. 1950.

[6] Maeder, P.F., "Investigation of the Boundary Condition at a Perforated Wall," Division of Engineering, Brown University, Providence, R.I., Tech. Rept. WT-9, May 1953.

[7] Chew, W.L., "Cross-Flow Calibration at Transonic Speeds of Fourteen Perforated Plates with Round Holes and Airflow Parallel to the Plates," AEDC-TR-54-65, July 1955.

[8] Chew, W.L., "Characteristics of Perforated Plates with Conventional and Differential Resistance to Cross-Flow and Airflow Parallel to the Plates," *Proceedings of the Propulsion Wind Tunnel Transonic Seminar: Vol. I, Discussion of Transonic Testing Problems,* AEDC, 1956.

[9] Lukasiewicz, J., "Effects of Boundary Layer and Geometry on Characteristics of Perforated Walls for Transonic Wind Tunnels," Vol. 20, *Aerospace Engineering,* April 1961, pp. 22–23, 62–68.

[10] Ohman, L.H., "The NAE High Reynolds Number 15″ × 60″ Two-Dimensional Test Facility: Part I, General Information," National Aeronautical Establishment, Laboratory Tech. Rept. LTR-HA-4, April 1974.

[11] Kacprzynski, J.J., Ohman, L.H., Garabedian, P.R., and Korn, D.G., "Analysis of the Flow Past a Shockless Lifting Airfoil In-Design and Off-Design Conditions," National Research Council of Canada, Aero Rept. LR-554, Nov. 1971.

[12] Van Driest, E.R., "Convective Heat Transfer in Gases," *Turbulent Flows and Heat Transfer,* edited by C.C. Lin, Princeton University Press, Princeton, N.J., 1959.

[13] Chan, Y.Y., "Boundary Layer Development on Perforated Walls in Transonic Wind Tunnels," National Aeronautical Establishment, Ottawa, Canada, Laboratory Tech. Rept. LTR-HA-47, Feb. 1980.

[14] Chan, Y.Y., "Compressible Turbulent Boundary Layer Computations Based on Extended Mixing Length Approach," *Canadian Aeronautical and Space Institute Transactions,* Vol. 5, No. 1, March 1972, pp. 21–27.

[15] Fannelop, T.K., "Displacement Thickness for Boundary Layers with Surface Mass Transfer," *AIAA Journal,* Vol. 4, June 1966, pp. 1142–1144.

[16] Jones, D.J., Private communication, Oct. 1979.

[17] Mokry, M., Peake, D.J., and Bowker, A.J., "Wall Interference on Two-Dimensional Supercritical Airfoils, Using Wall Pressure Measurements to Determine the Porosity Factors for Tunnel Floor and Ceiling," National Research Council of Canada, NRC/NAE Aero. Rept. LR-575, Feb. 1974.